Article

Cell Reports

Genomic Location of PRMT6-Dependent H3R2 Methylation Is Linked to the Transcriptional Outcome of Associated Genes

Graphical Abstract

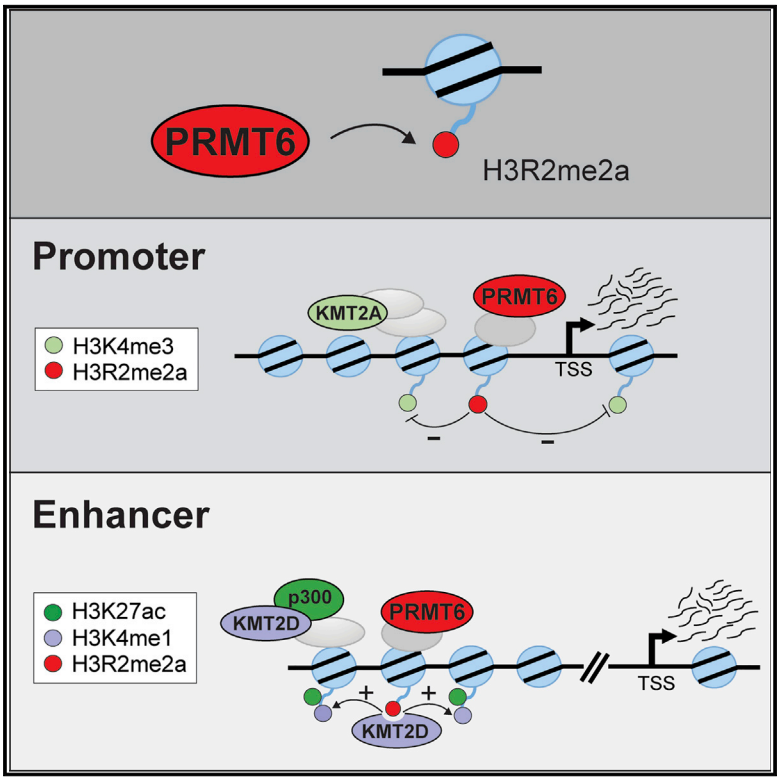

Highlights

- PRMT6 deposits H3R2me2a at promoters as well as enhancers of active genes
- H3R2me2a influences the occurrence of adjacent histone marks (H3K4me3, H3K4me1, H3K27ac)
- H3R2me2a contributes to gene repression at promoters and gene activation at enhancers
- PRMT6/H3R2me2a modulate the transcription of important neural differentiation genes

Authors

Caroline Bouchard, Peeyush Sahu, Marion Meixner, ..., Thorsten Stiewe, Sjaak Philipsen, Uta-Maria Bauer

Correspondence

bauer@imt.uni-marburg.de

In Brief

Bouchard et al. identify the genome-wide, PRMT6-dependent occurrence of H3R2me2a in a cell model of neural differentiation. H3R2me2a is localized at promoters and enhancers of active genes and influences the chromatin recruitment of histone lysine methyltransferases. Thereby, H3R2me2a modulates the deposition of adjacent histone H3 marks and regulates the transcriptional output of genes relevant for pluripotency and differentiation.

Data and Software Availability

GSE107612

Bouchard et al., 2018, Cell Reports *24*, 3339–3352
September 18, 2018
https://doi.org/10.1016/j.celrep.2018.08.052

CellPress

Cell Reports
Article

Genomic Location of PRMT6-Dependent H3R2 Methylation Is Linked to the Transcriptional Outcome of Associated Genes

Caroline Bouchard,[1,12] Peeyush Sahu,[1,12] Marion Meixner,[1,12] René Reiner Nötzold,[1,12] Marco B. Rust,[2] Elisabeth Kremmer,[3] Regina Feederle,[4] Gene Hart-Smith,[5] Florian Finkernagel,[6] Marek Bartkuhn,[7] Soni Savai Pullamsetti,[8] Andrea Nist,[9] Thorsten Stiewe,[9,10] Sjaak Philipsen,[11] and Uta-Maria Bauer[1,13,*]

[1]Institute for Molecular Biology and Tumor Research (IMT), Philipps-University Marburg, Hans-Meerwein-Strasse 2, BMFZ, 35043 Marburg, Germany
[2]Molecular Neurobiology Group, Institute of Physiological Chemistry, Philipps-University Marburg, Karl-von-Frisch-Strasse 1, 35043 Marburg, Germany
[3]Institute of Molecular Immunology, Helmholtz Zentrum München, German Research Center for Environmental Health GmbH, 81377 Munich, Germany
[4]Monoclonal Antibody Core Facility, Institute for Diabetes and Obesity, Helmholtz Zentrum München, German Research Center for Environmental Health GmbH, Ingolstädter Landstrasse 1, 85764 Neuherberg, Germany
[5]School of Biotechnology and Biomolecular Sciences, University of New South Wales, Sydney, New South Wales 2052, Australia
[6]Center for Tumor Biology and Immunology (ZTI), Philipps-University Marburg, Hans-Meerwein-Strasse 3, 35043 Marburg, Germany
[7]Institute for Genetics, Justus-Liebig-University Giessen, Heinrich-Buff-Ring 58-62, 35392 Giessen, Germany
[8]Department of Lung Development and Remodeling, Max-Planck-Institute for Heart and Lung Research, Member of the German Center for Lung Research (DZL), Bad Nauheim, Germany
[9]Genomics Core Facility, Philipps-University Marburg, Hans-Meerwein-Strasse 3, 35043 Marburg, Germany
[10]Institute of Molecular Oncology, Philipps-University Marburg, Hans-Meerwein-Strasse 3, 35043 Marburg, Germany
[11]Department of Cell Biology, Erasmus MC, Rotterdam, the Netherlands
[12]These authors contributed equally
[13]Lead Contact
*Correspondence: bauer@imt.uni-marburg.de
https://doi.org/10.1016/j.celrep.2018.08.052

SUMMARY

Protein arginine methyltransferase 6 (PRMT6) catalyzes asymmetric dimethylation of histone H3 at arginine 2 (H3R2me2a). This mark has been reported to associate with silent genes. Here, we use a cell model of neural differentiation, which upon PRMT6 knockout exhibits proliferation and differentiation defects. Strikingly, we detect PRMT6-dependent H3R2me2a at active genes, both at promoter and enhancer sites. Loss of H3R2me2a from promoter sites leads to enhanced KMT2A binding and H3K4me3 deposition together with increased target gene transcription, supporting a repressive nature of H3R2me2a. At enhancers, H3R2me2a peaks colocalize with the active enhancer marks H3K4me1 and H3K27ac. Here, loss of H3R2me2a results in reduced KMT2D binding and H3K4me1/H3K27ac deposition together with decreased transcription of associated genes, indicating that H3R2me2a also exerts activation functions. Our work suggests that PRMT6 via H3R2me2a interferes with the deposition of adjacent histone marks and modulates the activity of important differentiation-associated genes by opposing transcriptional effects.

INTRODUCTION

A multitude of nuclear and cytoplasmic proteins are posttranslationally modified by arginine methylation. Arginines frequently contribute to intermolecular interactions due to hydrogen-bonding and amino-aromatic interactions. Methylation of such pivotal arginine residues modulates the binding affinity between interaction partners leading to promotion or inhibition of interactions (Gayatri and Bedford, 2014). The enzymes responsible for this modification are protein arginine methyltransferases (PRMTs), which constitute an enzyme family of nine members in mammals (Yang and Bedford, 2013). They transfer methyl groups from the ubiquitous methyl-group donor *S*-adenosyl-L-methionine (SAM) to the terminal guanidino nitrogens of arginine residues, giving rise to monomethyl-arginine (MMA), asymmetric dimethyl-arginine (ADMA), or symmetric dimethyl-arginine (SDMA). PRMTs regulate a wide range of essential cellular processes, for example, signal transduction, nucleo-cytoplasmic transport, transcriptional regulation, RNA splicing, and DNA repair (Yang and Bedford, 2013).

Our previous studies identified asymmetric dimethylation of histone H3 at arginine 2 (H3R2me2a) as the predominant histone mark catalyzed by the family member PRMT6 (Hyllus et al., 2007). H3R2me2a was found to contribute to gene repression by blocking the catalytic activity of the H3K4 methyltransferase KMT2A and counteracting the formation of H3K4 trimethylation (Guccione et al., 2007; Hyllus et al., 2007; Iberg et al., 2008;

Kirmizis et al., 2007; Michaud-Levesque and Richard, 2009; Stein et al., 2012). In agreement with these observations, H3R2me2a was shown to be depleted from active genes and present at genomic regions with low H3K4me3 occupancy, such as silent genes and heterochromatin (Barski et al., 2007; Rosenfeld et al., 2009). Transcriptional repression by PRMT6 and H3R2me2a was reported to be relevant for pluripotency, differentiation processes, as well as maintenance of fully differentiated cells in various tissues (Dhawan et al., 2011; Lee et al., 2012; Stein et al., 2016). Given that until now our understanding of the gene-regulatory functions of H3R2me2a derived from analyses of individual genes and subsets of genomic loci, we investigated here the PRMT6-dependent transcriptome and genomic distribution of H3R2me2a in an unbiased and genome-wide manner. Moreover, we studied the putative cross talk between H3R2me2a and neighboring histone marks, such as H3K4 methylation (H3K4me1 and H3K4me3), H3K27 methylation (H3K27me3), and H3K27 acetylation (H3K27ac).

For these studies, we used the human embryonal carcinoma cell line NT2/D1, which is pluripotent and differentiates into neural precursor cells upon treatment with *all-trans* retinoic acid (ATRA) (Lee and Andrews, 1986). We chose this model since PRMT6 knockdown causes alterations in the transcriptional program of undifferentiated as well as ATRA-induced NT2/D1 cells (Hyllus et al., 2007; Stein et al., 2016). PRMT6 wild-type and knockout NT2/D1 cells were employed in chromatin immunoprecipitation-sequencing (ChIP-seq) and RNA-sequencing (RNA-seq) analyses. In contrast to our expectations, we found that H3R2me2a is deposited in a PRMT6-dependent manner primarily at active genes, both at promoter and enhancer sites. Here, H3R2me2a seems to contribute to the transcriptional regulation of important pluripotency and differentiation-associated genes by influencing the deposition of neighboring histone marks. Our data support the concept that arginine methylation exerts its regulatory activity by modulating protein-protein interactions. Depending on its genomic location, H3R2me2a possesses either a repressive or activating nature: transcriptional repression at promoters and transcriptional activation at enhancers.

RESULTS

PRMT6-Dependent H3R2me2a Is Predominantly Deposited at TSS and Promoter Regions in Undifferentiated NT2/D1 Cells

By combining genome-wide analyses on the H3R2me2a deposition profile (ChIP-seq) and the PRMT6-dependent transcriptome (RNA-seq), we aimed to elucidate the functional and mechanistic impact of PRMT6 and its major histone mark in gene regulation. We used CRISPR/Cas9 genome editing to generate PRMT6 knockout (KO) and control (CT) NT2/D1 cells. NT2/D1 KO cell lines showed a complete loss of PRMT6 expression and a global reduction of arginine methylated proteins in comparison to CT cells (Figure 1A). Furthermore, we generated an antibody, which specifically recognizes the H3R2me2a modification, also in presence of the neighboring H3K4me3 mark (Figures S1A–S1E). Monomethylated H3R2 (H3R2me1) was weakly detected by the antibody, whereas unmethylated H3R2 (H3R2me0), symmetrically dimethylated H3R2 (H3R2me2s), and other methylation marks of the H3 as well as H4 N terminus were not recognized (Figures S1A–S1E). We performed ChIP-seq using this antibody and obtained in undifferentiated NT2/D1 CT cells a total of 2,300 binding sites, as visualized by heatmap (Figure 1B). In contrast, ChIP-seq datasets of two NT2/D1 KO cell lines revealed a strong reduction of H3R2me2a signals indicating that these 2,300 sites are PRMT6 dependent (Figures 1B and S1F). Analysis of the relative genomic distribution of the H3R2me2a sites showed that 72% of these occur in the vicinity of transcriptional start sites (TSSs) (Figure 1C). To validate these ChIP-seq results, we selected candidate loci, as depicted in the genome browser views for NT2/D1 CT and KO cells (Figures 1D and S1G). Using independent ChIP-qPCR assays, we confirmed the H3R2me2a occupancy at these loci in undifferentiated NT2/D1 CT cells as well as the loss of H3R2me2a enrichment upon PRMT6 deletion (Figures 1E and S1H). Control regions in proximity to H3R2me2a binding sites revealed background signal of H3R2me2a in NT2/D1 CT and KO cells (Figure 1E). Native ChIP analysis in CT cells reproduced the H3R2me2a binding sites (Figure S1I). Furthermore, re-expression of PRMT6 in KO cells resulted in the re-establishment of H3R2me2a occupancy (Figures S2A–S2D). Hence, these results uncover the genome-wide binding profile of PRMT6-dependent H3R2me2a in pluripotent NT2/D1 cells. The predominant TSS and promoter-proximal distribution of H3R2me2a suggests that this mark is likely involved in the regulation of gene expression.

H3R2me2a Deposition Displays Three Distinct Patterns during ATRA-Induced NT2/D1 Cell Differentiation

Next, we analyzed the dynamics of H3R2me2a deposition during NT2/D1 cell differentiation upon ATRA treatment. A total of 8,819 unique H3R2me2a binding sites was detected by ChIP-seq in undifferentiated and differentiated NT2/D1 CT cells, which encompassed the 2,300 peaks of undifferentiated cells and additional 6,519 peaks acquired upon differentiation. Based on their enrichment in the minus-ATRA and plus-ATRA conditions, we divided these peaks into three clusters (Figure 2A). Cluster I peaks are present in the minus-ATRA condition and are reduced or lost upon ATRA treatment, cluster II peaks are equally strong in both ATRA conditions, and cluster III peaks show a gain of H3R2me2a enrichment upon ATRA-induced differentiation. In NT2/D1 KO cells, the peaks of all three clusters were significantly reduced (Figure 2A). Using gene ontology (GO) analysis, we found that genes associated with the three different peak clusters execute distinct and essential functions in NT2/D1 cells (Figure 2B). Cluster I-associated genes were predominantly annotated to terms such as axon guidance, stem cell maintenance, and pluripotency, as exemplified by the genes *OCT4*, *NANOG*, *ID1*, and *REST*, which are downregulated upon neural differentiation (Figure 2B). Cluster II genes, e.g., *ST3GAL2*, *MITF*, *FASTKD1*, *CNOT1*, and *LARS*, revealed as overrepresented GO terms cell cycle, RNA processing, chromatin organization, DNA damage response, and posttranslational modifications (PTMs). These peaks showed particularly robust enrichment, as validated in Figure 1E, and associate with genes that are not responsive to ATRA treatment (Figure 2B). In cluster III, the overrepresented GO terms were cell cycle, CNS development, and neurogenesis. Gene examples are the *HOXA* cluster, *RARB*, *VTCN1*, *CRABP1*, and

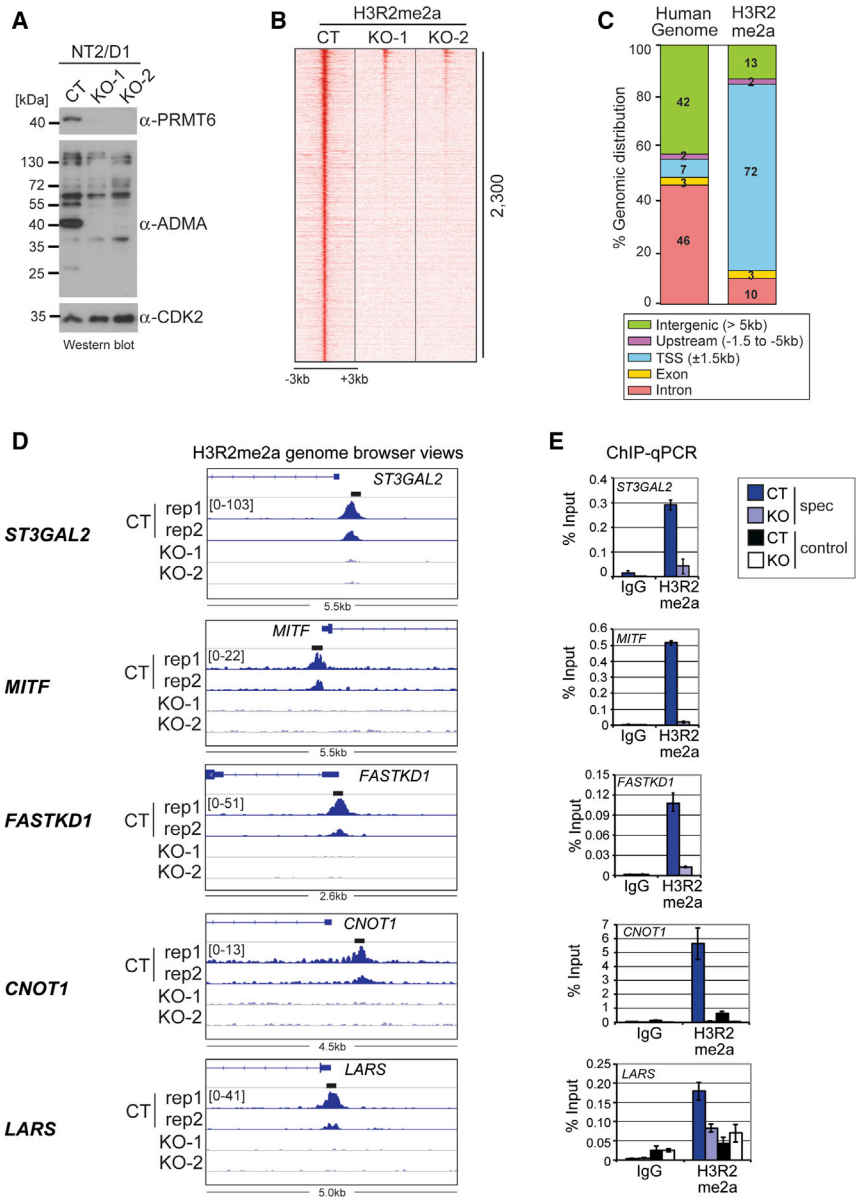

Figure 1. PRMT6-Dependent and Promoter-Proximal Deposition of H3R2me2a in NT2/D1 Cells

(A) Protein extracts of undifferentiated control (CT) or PRMT6-deleted (KO-1, KO-2) NT2/D1 cell lines were analyzed by western blot using the indicated antibodies (α-PRMT6, α-ADMA, α-CDK2). CDK2 staining served as loading control. Size markers (in kilodaltons) are shown on the left.

(B) Heatmap displays the H3R2me2a ChIP-seq signals in undifferentiated NT2/D1 CT cells over the 2,300 binding sites sorted in the descending order of their signal strength (±3 kb around the centered summits) in comparison to H3R2me2a ChIP-seq profiles of NT2/D1 KO-1 and KO-2 cell lines.

(C) Relative distribution of the 2,300 H3R2me2a peaks (of B) is shown within different genomic regions compared to the distribution of these regions in the human genome.

(D) Genome browser views of H3R2me2a ChIP-seq datasets of NT2/D1 CT (two replicates) and both KO cell lines are shown for five gene loci. Positions of amplicons (spec, specific region) generated by qPCR (E) are depicted as black boxes above the top browser tracks. Data range is indicated in brackets.

(E) ChIP-qPCR assays were performed in NT2/D1 CT and KO cells (=KO-2, which we employed in all subsequent experiments as PRMT6 knockout cell line) using control antibodies (IgG) and α-H3R2me2a. Precipitated DNA was analyzed by qPCR with primers amplifying the H3R2me2a peaks (spec) or a nearby control region (control) of the depicted loci. Amplicons for control regions are in case of *CNOT1* 16 kb downstream of TSS in intron 1 and in case of *LARS* 18 kb downstream of TSS in exon 6. Recruitment is displayed in percent input of chromatin; mean ± SD of triplicates.

ARID1A, which are predominantly upregulated upon ATRA treatment (Figure 2B). In ChIP-qPCR and RT-qPCR assays, we validated several candidate genes of the three clusters for their H3R2me2a occupancy and transcriptional characteristics in undifferentiated and ATRA-treated NT2/D1 CT cells, such as *OCT4* and *ID1* for cluster I, *LARS* and *MITF* for cluster II, and *VTCN1* and *CRABP1* for cluster III (Figures 2C and S3A). These results demonstrate that H3R2me2a displays differentiation-dependent dynamics in NT2/D1 cells and marks genes, which exert essential functions in pluripotency, cell cycle, and neural differentiation.

H3R2me2a Co-localizes with Other Histone H3 Marks and Associates with Active Genes

Given that H3R2me2a has been reported to influence the occurrence of adjacent histone H3 modifications, in particular H3K4me3 (Guccione et al., 2007; Hyllus et al., 2007), we analyzed the distribution of this promoter mark in undifferentiated and differentiated NT2/D1 CT cells by ChIP-seq. Surprisingly, we found that 48% (4,236 peaks) of the total 8,819 H3R2me2a sites overlap with a high occupancy of H3K4me3 but not with H3K27me3, suggesting that H3R2me2a is mainly present at non-bivalent, active gene promoters (Figures 2D, S3B, and S3C). No global changes in the H3K4me3 occupancy were observed when comparing minus/plus-ATRA conditions. Genes of all three clusters contributed to this group of promoter-associated H3R2me2a peaks. The remaining 4,538 H3R2me2a sites displayed very low occupancy of H3K4me3 (Figure 2D) and high enrichment of non-TSS regions (data not shown). This prompted us to examine the distribution of two enhancer modifications, H3K4me1 and H3K27ac. H3K4me1 alone marks primed enhancers, whereas H3K4me1 in conjunction with H3K27ac characterizes active enhancers (Calo and Wysocka, 2013). Interestingly, we observed that the remaining 52% H3R2me2a binding sites predominantly co-occur with sites of high H3K4me1 and H3K27ac occupancy,

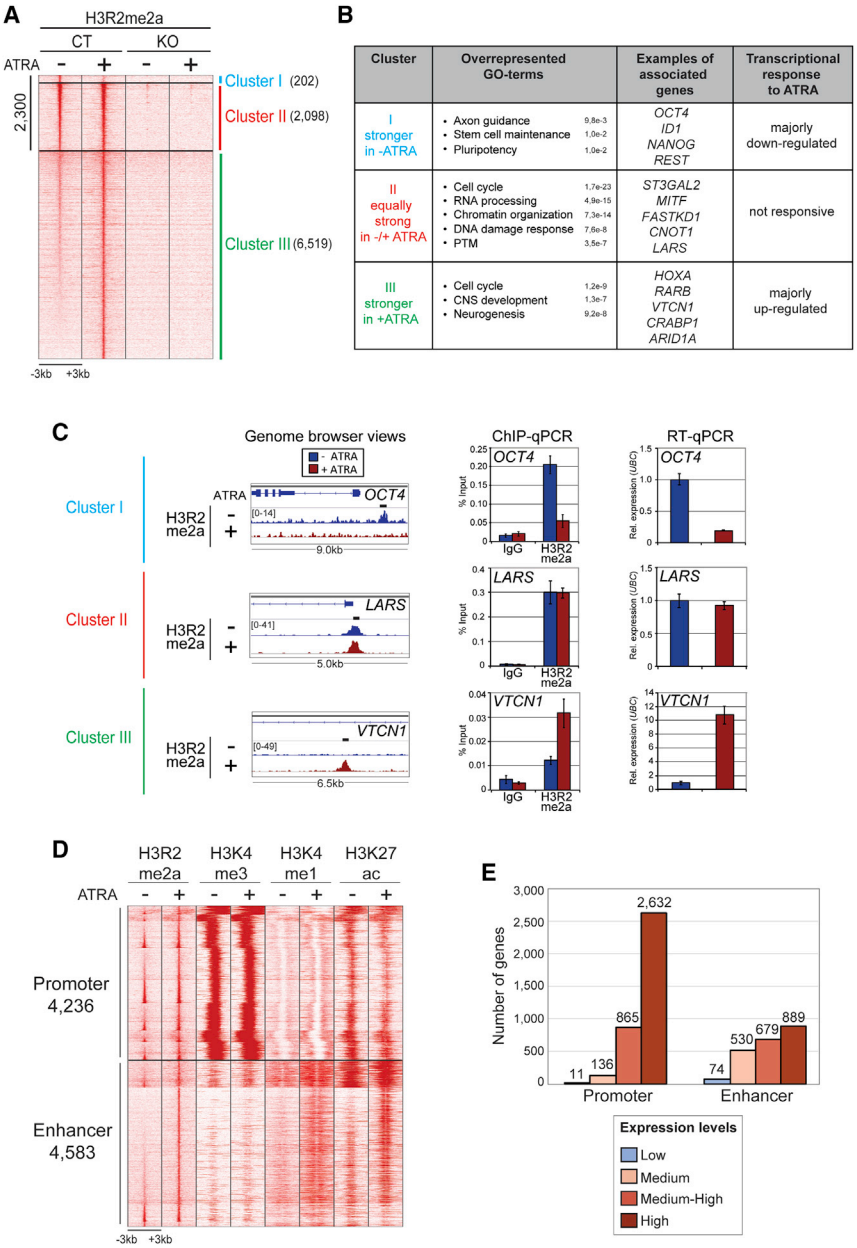

Figure 2. Dynamics of the Genome-wide H3R2me2a Deposition during NT2/D1 Cell Differentiation and Co-occurrence of H3R2me2a with Other Histone H3 Marks

(A) Heatmap of H3R2me2a ChIP-seq binding profile (±3 kb around the centered peak summits) in NT2/D1 CT versus KO cells minus/plus ATRA at 8,819 genomic loci. Peaks are divided into three clusters (I, II, and III) depending on their H3R2me2a enrichment in the minus- and plus-ATRA conditions.

(B) Table summarizing the characteristics of genes associated with H3R2me2a binding sites of the three clusters. Overrepresented GO terms and their corresponding q values are indicated.

(C) Genome browser views of the H3R2me2a ChIP-seq datasets of NT2/D1 CT cells minus/plus ATRA are depicted for gene loci illustrating the three clusters (left panels): *OCT4* (cluster I), *LARS* (cluster II), and *VTCN1* (cluster III). Positions of amplicons generated by qPCR are depicted as black boxes above the top browser tracks. Data range is indicated in brackets. ChIP-qPCR assays were performed using control antibodies (IgG) and α-H3R2me2a and primers amplifying the H3R2me2a peaks of the depicted loci. Recruitment is displayed in percent input of chromatin; mean ± SD of triplicates (middle panels). Total RNA was analyzed by RT-qPCR for the transcript levels derived from three gene loci. Values were normalized to *UBIQUITIN* (*UBC*) expression and presented relative to the minus-ATRA condition; mean ± SD of triplicates (right panels).

(D) Heatmap displays the H3R2me2a ChIP signals over 8,819 sites in comparison to ChIP-seq profiles of histone marks (H3K4me3, H3K4me1, and H3K27ac) in NT2/D1 CT cells minus/plus ATRA, as regions classified in promoters (4,236 sites) or enhancers (4,583 sites) based on the signal strength of their specific histone marks.

(E) RNA-seq analysis was performed in NT2/D1 CT cells plus ATRA. Genes associated with H3R2me2a binding sites either at their promoter or enhancer were binned according to their transcriptional strength in four categories based on expression quantiles (normalized as TPM [transcript per million reads per kilobase]): low, <0.09 and >0; medium, <0.84 and ≥0.09; medium-high, <10.5 and ≥0.84; high, >10.5.

indicating that here H3R2me2a localizes with active enhancer regions (Figure 2D). These enhancer-associated H3R2me2a binding sites showed an increase in H3K4me1 and H3K27ac occupancy concomitant to the gain in H3R2me2a enrichment upon ATRA treatment. Over 80% of the H3R2me2a enhancer sites belong to cluster III. To address whether the here-observed H3R2me2a deposition feature is a cell-type-specific phenomenon, we performed ChIP-seq analysis of this mark in the human osteosarcoma cell line U2OS with either wild-type levels of PRMT6 (CT) or PRMT6 KO. Thereby, we identified 3,253 PRMT6-dependent H3R2me2a sites, of which 47% (1,556 peaks) overlapped with peaks in NT2/D1 cells (Figures S4A–S4F). Interestingly, as observed in NT2/D1 cells, H3R2me2a sites in U2OS cells were co-occupied by H3K4me3 or H3K4me1/H3K27ac (Figure S4G). Thus, our results indicate that the co-occurrence of H3R2me2a with these other H3 marks is a general and cell-type-independent characteristic.

To determine the transcriptional output of genes with either promoter- or enhancer-deposited H3R2me2a in NT2/D1 cells, we performed RNA-seq analyses. We then binned all H3R2me2a-associated unique genes (6,697) according to their transcription levels in differentiated CT cells. We found that H3R2me2a at promoters predominantly marks highly transcribed genes, whereas H3R2me2a at enhancers is located in proximity to genes distributed in all four categories of expression levels (Figure 2E). Our observations were unexpected, since up

to now PRMT6 and H3R2me2a have been reported to mainly associate with silent genes (Guccione et al., 2007; Hyllus et al., 2007; Iberg et al., 2008; Kirmizis et al., 2007). Altogether, these results reveal that H3R2me2a possesses two distinct locations in the genome, at promoter and enhancer sites. At both locations, H3R2me2a co-occurs with active histone modifications and consistently marks primarily active genes.

H3R2me2a Contributes to Activation as well as Repression of Associated Genes

To address whether H3R2me2a influences the transcriptional output of the associated genes, we compared the PRMT6-dependent transcriptome of NT2/D1 CT and KO cells by RNA-seq. We identified 710 differentially expressed genes in ATRA-stimulated cells (Figure S5A). These deregulated genes were almost equally distributed into the upregulated and downregulated groups, respectively (374 upregulated genes and 336 downregulated genes). To distinguish direct from indirect transcriptional effects of PRMT6-dependent H3R2me2a, we combined our ChIP-seq and RNA-seq datasets. This analysis showed that approximately 25% of deregulated genes (176 genes) harbor H3R2me2a binding sites in their proximity. A larger number of genes with enhancer-deposited H3R2me2a was deregulated compared to genes with promoter-deposited H3R2me2a (Figure S5B). The majority of these direct H3R2me2a targets (70%) were downregulated upon PRMT6 knockout, indicating that PRMT6-dependent H3R2me2a predominantly contributes to transcriptional activation of associated genes. This effect was more pronounced for genes associated with H3R2me2a enhancer peaks (Figure S5B). Altogether, our results indicate that H3R2me2a contributes to gene repression as well as gene activation, the latter accounting for the majority of effects.

Promoter-Associated H3R2me2a Attenuates H3K4me3 Occupancy and Transcriptional Activity

We next investigated whether promoter-associated H3R2me2a influences the deposition of H3K4me3 and the transcriptional output of the associated genes. Thus, we plotted the intensity of H3K4me3 signals in NT2/D1 CT versus KO cells and found that the H3K4me3 occupancy of upregulated genes is significantly increased upon PRMT6 knockout (Figures 3A and S5C). On the contrary, the downregulated genes showed no significant difference in the H3K4me3 deposition between CT and KO cells. Our findings suggest that PRMT6 and H3R2me2a negatively influence H3K4me3 deposition at the chromatin. Independent ChIP-qPCR verified the higher occupancy of H3K4me3 for genes of all three clusters in PRMT6-deficient cells (Figures 3B and S5D). Moreover, this increase in H3K4me3 occupancy coincided with an elevated transcriptional activity (Figures 3C and S5D) and an enhanced KMT2A binding to these H3R2me2a target genes in KO cells (Figure 3D). Our data indicate that promoter-associated H3R2me2a possesses a repressive nature by interfering with the recruitment of KMT2A and antagonizing the deposition of H3K4me3. However, in contrast to previous perceptions (Guccione et al., 2007; Hyllus et al., 2007; Iberg et al., 2008), this repressive function of H3R2me2a does not occur at silent gene loci, but rather at active genes, causing a restraint of their transcriptional output. Thus, H3R2me2a localized at promoters leads to fine-tuning of transcriptional activities and impedes unauthorized high expression of pluripotency genes (cluster I, Figure 2B) as well as differentiation-associated genes (cluster III, Figure 2B) in NT2/D1 cells.

Enhancer-Associated H3R2me2a Promotes the Deposition of H3K4me1/H3K27ac and the Transcriptional Activation of Corresponding Genes

To investigate the role of enhancer-associated H3R2me2a binding sites, we plotted these peaks according to their affiliation to cluster I, II, and III in NT2/D1 CT and KO cells and compared them to the ChIP-seq profiles of H3K4me3, H3K4me1, and H3K27ac (Figure 4A). As mentioned above, enhancer-associated H3R2me2a peaks mainly belong to cluster III (i.e., increased peak intensity in plus ATRA) and generally show very low occupancy of H3K4me3. Strikingly, deposition of H3K4me1 and H3K27ac resembled the occurrence of H3R2me2a at cluster III genes. The occupancy of both enhancer marks clearly augmented upon differentiation of NT2/D1 CT cells (comparing CT minus/plus ATRA, Figures 4A and 4B). This ATRA-induced increase was significantly diminished upon deletion of PRMT6 (comparing CT and KO, both plus ATRA), suggesting that the differentiation-associated depositions of H3R2me2a and the two enhancer marks are connected. This assumption was supported by the facts that PRMT6 knockout had a very moderate impact on the H3K4me1/H3K27ac occupancy in undifferentiated cells (comparing CT and KO, both minus ATRA), and further that the ATRA-induced increased deposition of enhancer marks was only marginally detectable in KO cells (comparing KO minus/plus ATRA, Figures 4A and 4B). Moreover, we observed a strong positive correlation between the enrichment levels of H3R2me2a and both enhancer marks in differentiating CT cells (Figures S6A and S6B). Collectively, our findings point to an H3R2me2a-dependent deposition mechanism of these enhancer histone marks.

The H3K4 mono-methyltransferase KMT2D contains several PHD fingers, of which PHD_{4-6} are well-known reader domains of histone H4 (Dhar et al., 2012). We investigated here whether KMT2D also binds to the histone H3 tail and whether this binding is influenced by H3R2me2a. Therefore, we performed peptide pull-down assays using either recombinant GST-KMT2D purified from bacteria or Flag-KMT2D overexpressed in cell lysates. By means of wild-type and mutant KMT2D proteins, we found that PHD_{4-6} of KMT2D, in particular PHD_6, possess binding preferences for H3R2me1 and H3R2me2a peptides, but not for H3R2me0, H3R2me2s, or H3R17me2a (Figures 4C, S6C, and S6D). In agreement with these findings, ChIP-seq analysis of KMT2D in NT2/D1 CT and KO cells showed a co-occurrence of H3R2me2a and KMT2D (Figures 4A, 4B, and S6E–S6I). Furthermore, we detected a positive correlation of H3R2me2a and KMT2D enrichment levels at the chromatin and, importantly, a dependence of KMT2D binding on H3R2me2a deposition (Figures S6G–S6I). Our data suggest that PRMT6 facilitates the deposition of H3K4me1 potentially in a direct manner by enhancing chromatin recruitment of the KMT2D complex, which has been reported to promote p300-dependent H3K27 acetylation (Wang et al., 2016, 2017).

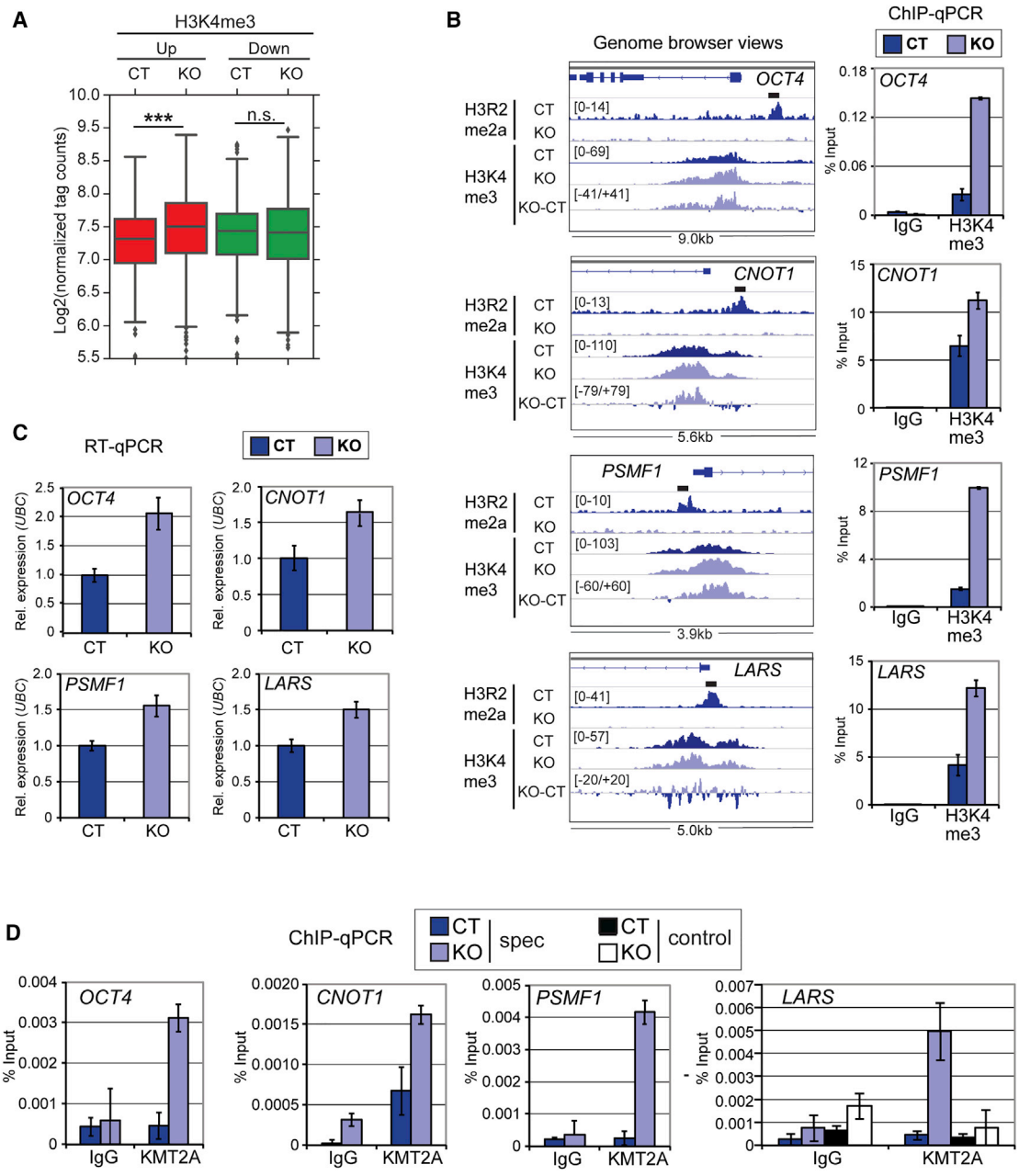

Figure 3. Negative Influence of Promoter-Associated H3R2me2a on H3K4me3 Deposition and Transcriptional Activity of Target Genes

(A) Boxplot analysis presents the normalized H3K4me3 tag counts for upregulated (red boxes) and downregulated genes (green boxes) in NT2/D1 CT and KO cells. ***p $\leq$ 0.001; n.s.: not significant using Welch's t test.

(B) Genome browser views of the H3R2me2a and H3K4me3 ChIP-seq datasets generated in NT2/D1 CT and KO cells are shown for the indicated gene loci (left panels). H3K4me3 signal differences between NT2/D1 KO and CT are illustrated in a separate track (KO-CT). Positions of amplicons generated by qPCR are depicted as black boxes above the top browser tracks. Data range is indicated in brackets. ChIP-qPCR assays were performed in NT2/D1 CT and KO cells using control antibodies (IgG) or α-H3K4me3 and primers encompassing the H3R2me2a peaks of the different loci. Recruitment is displayed in percent input of chromatin; mean ± SD of triplicates (right panels).

(C) Total RNA of NT2/D1 CT and KO cells was analyzed by RT-qPCR for transcript levels of the indicated genes (studied in B). Values were normalized to *UBIQUITIN* (*UBC*) expression and presented relative to NT2/D1 CT cells; mean ± SD of triplicates.

(D) ChIP-qPCR assays were performed in NT2/D1 CT and KO cells using control antibodies (IgG) or α-KMT2A and primers encompassing the H3R2me2a peaks (spec, specific region) of the different loci (studied in B) as well as a control region for *LARS* (=control; 18 kb downstream of TSS in exon 6). Recruitment is displayed in percent input of chromatin; mean ± SD of triplicates.

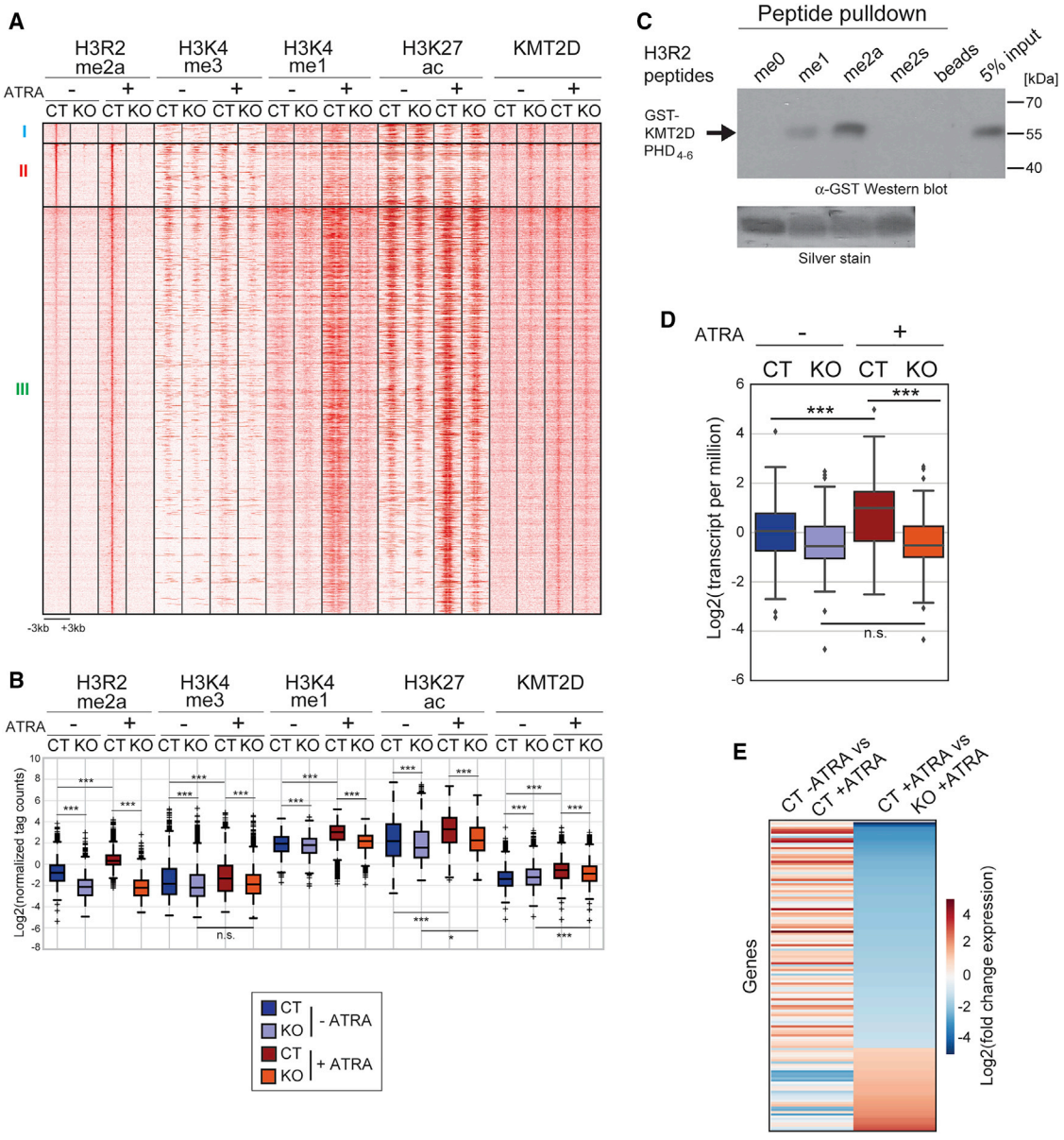

Figure 4. Promotion of H3K4me1 and H3K27ac Deposition by Enhancer-Associated H3R2me2a

(A) Heatmap presents the 4,583 enhancer-associated H3R2me2a binding sites in NT2/D1 CT cells minus/plus ATRA (as well as in KO cells) according to their affiliation to the three clusters and in comparison to H3K4me3, H3K4me1, H3K27ac, and KMT2D ChIP-seq profiles.

(B) Boxplot analysis illustrates the normalized tag counts ±2 kb centering H3R2me2a peaks for all samples of cluster III in (A). *$p \leq 0.05$; ***$p \leq 0.001$; n.s., not significant using Welch's t test.

(C) Indicated histone H3 peptides (aa 1–8) were covalently coupled to Sulfolink beads and incubated with bacterially expressed and purified GST-KMT2D PHD_{4-6} protein. Pull-down reactions and 5% input of GST-KMT2D deletion protein were resolved by SDS-PAGE and analyzed by α-GST western blot. Silver staining of the H3 peptides served as loading control.

(D) Boxplot analysis illustrates the transcriptional strength of the 137 deregulated genes upon PRMT6 knockout, which associate with H3R2me2a enhancer marks, in NT2/D1 CT and KO cells minus/plus ATRA. ***$p \leq 0.001$ using Welch's t test.

(E) Heatmap visualizes expression changes of genes from (D) upon ATRA treatment of NT2/D1 CT as well as KO cells.

Consequently, we next asked whether deposition of H3R2me2a at enhancer sites affects the transcription of associated genes. Therefore, we analyzed the transcript levels of the 137 genes, which were found deregulated upon PRMT6 deletion in plus-ATRA condition and associate with H3R2me2a in their enhancer region (Figure S5B). The majority of these H3R2me2 target genes, which belong to cluster III, showed an increased expression upon ATRA-induced differentiation in CT cells

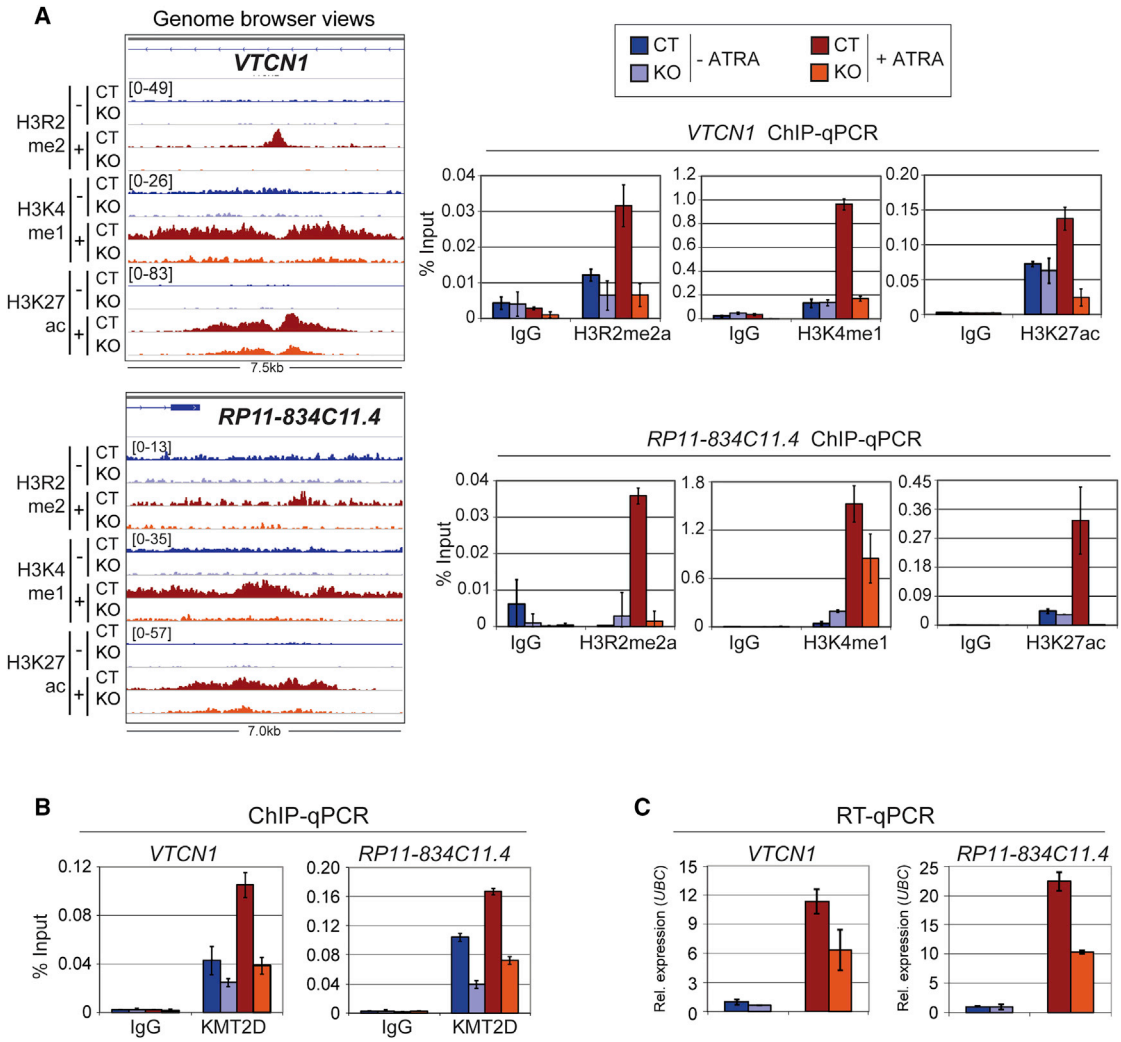

Figure 5. Transcriptional Activation Due to Enhancer-Associated H3R2me2a

(A) Genome browser views are shown for the indicated cluster III genes of H3R2me2a, H3K4me1, and H3K27ac ChIP-seq datasets generated in NT2/D1 CT and KO cells minus/plus ATRA (left panels). Data range is indicated in brackets. ChIP-qPCR assays were performed in NT2/D1 cells using the indicated antibodies and primers encompassing the histone modification peaks of the different loci. Recruitment is displayed in percent input of chromatin; mean ± SD of triplicates (right panels).

(B) ChIP-qPCR assays, as described in (A), were performed for KMT2D in NT2/D1 cells. The color code of the four conditions is displayed in (A).

(C) Transcript levels of the indicated cluster III genes (studied in A) were analyzed by RT-qPCR in NT2/D1 CT and KO cells minus/plus ATRA. The color code of the four conditions is displayed in (A). Values were normalized to *UBIQUITIN* (*UBC*) expression and presented relative to NT2/D1 CT cells minus ATRA; mean ± SD of triplicates.

(comparing CT minus/plus ATRA, Figure 4D). In contrast, in KO cells, ATRA treatment did not result in any significant increase in transcript levels of these genes (comparing KO minus/plus ATRA, Figure 4D). Importantly, comparing CT and KO in plus ATRA, PRMT6 knockout led to a loss of the differentiation-dependent transcriptional activation (Figure 4D). Besides, a heatmap of these transcriptional changes revealed that the very same genes, which were activated upon ATRA treatment in CT cells, lost their transcriptional response upon PRMT6 knockout (Figure 4E). Independent ChIP-qPCR and RT-qPCR assays of candidate cluster III genes, such as *VTCN1*, *RP11-834C11.4*, and *CRABP1*, validated the effects of PRMT6 deletion on H3K4me1/H3K27ac deposition, KMT2D recruitment, as well as transcriptional output (Figures 5A–5C and S7A). Moreover, re-expression of PRMT6 in NT2/D1 KO cells (Figure S2A) resulted in a rescue of the ATRA-induced H3K27ac deposition and differentiation-dependent transcriptional activation of associated genes (Figure S7B). Hence, our findings reveal that enhancer-associated H3R2me2a is predominantly deposited in a differentiation-dependent manner in NT2/D1 cells. There, it possibly promotes the deposition of H3K4me1 and H3K27ac, by recruitment of KMT2D, and thus enables transcriptional activation upon neural differentiation.

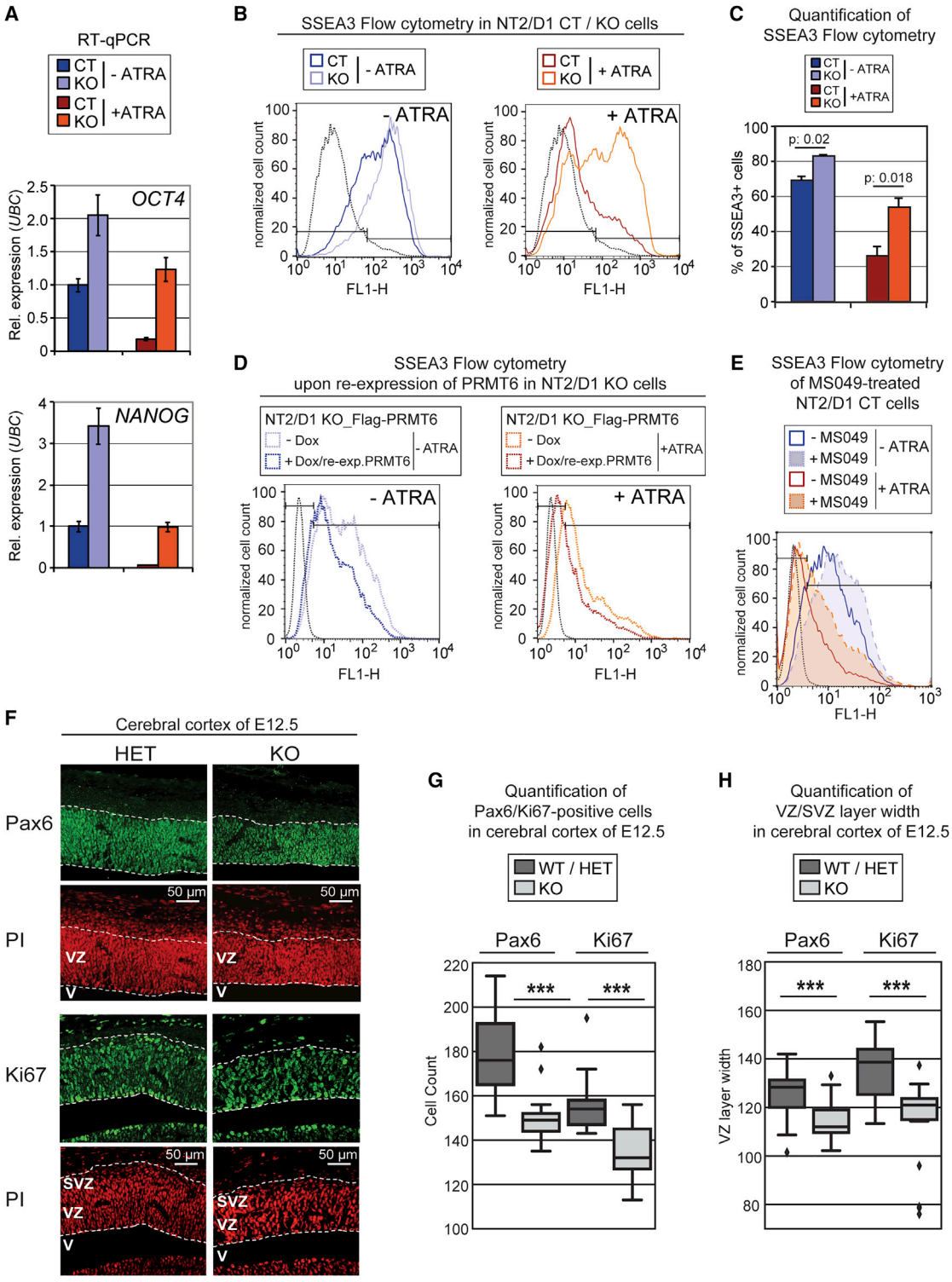

Figure 6. Impact of PRMT6 on Neural Differentiation and Proliferation *In Vitro* and *In Vivo*

(A) Transcript levels of *OCT4* and *NANOG* were analyzed by RT-qPCR in NT2/D1 CT versus KO cells minus/plus ATRA. Values were normalized to *UBIQUITIN* (*UBC*) expression and presented relative to NT2/D1 CT cells minus ATRA; mean ± SD of triplicates.

(B and C) The fraction of SSEA3-positive and SSEA3-negative cells was measured by flow cytometry of NT2/D1 CT and KO cells in minus- and plus-ATRA conditions. HeLa cells (black dotted line) served as negative control to define gates of SSEA3-positive and SSEA3-negative cells (black bars). (B) shows an

(legend continued on next page)

PRMT6 Influences the Differentiation and Proliferation Capacity of NT2/D1 Cells and of Neural Precursor Cells in the Developing Mouse Cortex

Given the enhanced expression of pluripotency-associated genes in NT2/D1 KO cells before and after ATRA treatment, as illustrated for *OCT4* and *NANOG* (Figure 6A), we raised the question whether PRMT6 influences the differentiation capacity of NT2/D1 cells. Undifferentiated NT2/D1 cells express the cell surface marker SSEA3, which indicates their stem cell-like state (Houldsworth et al., 2002). Using flow cytometry, we found that a higher percentage of NT2/D1 KO cells is SSEA3-positive and thus more pluripotent in the undifferentiated condition compared to CT cells (Figures 6B and 6C). Upon ATRA treatment, this difference was even more pronounced, suggesting that PRMT6 knockout leads to reduced neural differentiation. Additionally, undifferentiated NT2/D1 KO cells displayed a prolonged G1 phase and diminished proliferation rate (S phase) compared to CT cells, as measured by flow cytometry using propidium iodide staining (Figure S8A). These proliferation and differentiation defects of KO cells were rescued upon re-expression of PRMT6, which restored a higher number of cells in S phase, a reduced percentage of pluripotent (SSEA3-positive) cells in the minus-ATRA condition and an increased fraction of differentiating (SSEA3-negative) cells upon ATRA treatment (Figures 6D, S8B, and S8C). To further address whether the catalytic activity of PRMT6 is responsible for the neural differentiation phenotype of KO cells, we treated NT2/D1 CT cells with MS049, a potent PRMT6 inhibitor (Shen et al., 2016). This treatment resulted in a global reduction of arginine methylated proteins and a reduced genomic occupancy of H3R2me2a (Figures S8D–S8F). Interestingly, MS049 treatment phenocopied the defects on pluripotency and differentiation caused by PRMT6 knockout, indicating that these PRMT6-mediated functions require its catalytic activity (Figures 6E and S8G).

Since differentiating NT2/D1 cells resemble Pax6-positive neural stem cells of the developing fetal CNS (Houldsworth et al., 2002), we investigated whether Prmt6 also influences neural differentiation *in vivo* in mice. First, we analyzed the protein expression of Prmt6 in fetal and adult murine brain tissue. In agreement with previous studies, we found Prmt6 to be highly expressed in the developing mouse brain (McKee et al., 2005) as well as in different regions of the adult mouse brain (Figure S8H). Given that Pax6-positive as well as proliferating (Ki67-positive) neural progenitor cells are highly abundant in the mouse cerebral cortex of embryonic day 12.5 (E12.5), we quantified the progenitor numbers of this developmental stage in wild-type (WT) and heterozygous (HET) versus *Prmt6* KO mice (Neault et al., 2012). Thereby, we identified that the numbers of Pax6-positive and Ki67-positive progenitors, respectively, as well as the layer widths of the ventricular zone (VZ) and subventricular zone (SVZ) are reduced in the cerebral cortex of *Prmt6* KO embryos compared to WT and HET embryos (Figures 6F–6H). At later developmental stages and in the adult murine brain, we did not find significant differences in the number of neurons and in the morphology of the brain between WT/HET and KO animals (data not shown). Our observations are consistent with the inconspicuous phenotype of *Prmt6* KO mice (Neault et al., 2012). We hypothesize that the important *in vivo* functions of Prmt6 are partially compensated in the KO mouse model by other Prmt members. Hence, these findings show that PRMT6-deficient neural cells display a very stable stem cell-like state and a perturbation of their proliferation and differentiation capacity in an *in vitro* cell model as well as *in vivo*. Additional mechanisms involving non-catalytic functions and other substrates of PRMT6 could contribute to the here-described effects of PRMT6 knockout.

In summary, our data identify PRMT6 as a regulator of neural differentiation that seems to influence the transcription program of neural precursors, as exemplified here for NT2/D1 cells, at least in two ways: promoter-associated H3R2me2a diminishes the transcription of critical pluripotency genes, whereas enhancer-associated H3R2me2a promotes transcriptional activation of differentiation-associated genes.

DISCUSSION

To investigate the gene-regulatory functions of PRMT6 and its major histone mark H3R2me2a in an unbiased and genome-wide manner, we established CRISPR/Cas9-mediated deletion of PRMT6 in the human embryonal carcinoma cell line NT2/D1. In this well-established cell model, PRMT6 has previously been shown to regulate the ATRA-induced transcription program of

exemplary experiment. (C) displays the quantification of SSEA3-positive ($SSEA3^+$) cells of three independent experiments. The p values are indicated using Welch's t test.

(D) NT2/D1 KO_Flag-PRMT6 cells were cultured in the absence or presence of PRMT6 re-expression (minus/plus doxycycline for 6 days) and minus/plus ATRA (last 3 days). The fraction of SSEA3-positive and SSEA3-negative cells was measured by flow cytometry. HeLa cells (black dotted line) served as negative control to define gates of SSEA3-positive and SSEA3-negative cells (black bars). An exemplary experiment is shown. Quantification of four independent experiments is shown in Figure S8C.

(E) The fraction of SSEA3-positive and SSEA3-negative NT2/D1 CT cells either untreated or treated for 3 days with ATRA, MS049 (16 μM), or both was measured by flow cytometry. HeLa cells (black dotted line) served as negative control to define gates of SSEA3-positive and SSEA3-negative cells (black bars). An exemplary experiment is shown. Quantification of four independent experiments is shown in Figure S8G.

(F) Cryosections of the developing murine cerebral cortex of $Prmt6^{+/-}$ (HET) or $Prmt6^{-/-}$ (KO) embryos (E12.5) were stained by immunofluorescence for Pax6 (in green) as a neural progenitor cell marker, which recognizes the abundant number of apical radial glial cells of the murine ventricular zone (VZ) at this developmental stage, for Ki67 (in green) as a marker of the proliferating progenitors (predominantly in the VZ and SVZ [subventricular zone]) and for propidium iodide (PI) (in red) as a nuclear/DNA stain. The VZ (stained by Pax6) and the VZ/SVZ (stained by Ki67) are indicated between the white dotted lines and were taken into account for cell counting (G) and layer width quantification (H). The ventricles (V) are marked.

(G and H) For quantification of progenitor cell numbers as well as VZ and VZ/SVZ layer width in the murine cerebral cortex of E12.5, Pax6- and Ki67-positive cells, respectively, of a standardized area were determined in a blinded way from five to six $Prmt6^{+/+}$ (WT) or $Prmt6^{+/-}$ (HET) and six $Prmt6^{-/-}$ (KO) embryos. The cell numbers (G) and layer width (H) of WT/HET versus KO condition are depicted as boxplot. ***$p \leq 0.001$ using Welch's t test.

neural differentiation (Hyllus et al., 2007; Stein et al., 2016). Furthermore, PRMT6 is highly expressed in the developing mouse brain and has been suggested to influence the differentiation of embryonic stem cells (Lee et al., 2012; McKee et al., 2005). Recent studies disclosed a function of PRMT6 in the regulation of cocaine addiction in adult brain (Damez-Werno et al., 2016). Hence, using control and PRMT6 knockout NT2/D1 clones, we analyzed the impact of PRMT6-dependent H3R2me2a in pluripotency and neural differentiation. Here, PRMT6-deficient NT2/D1 cells displayed a slower growth rate compared to CT cells, in agreement with a higher number of cells in G1 phase and increased expression levels of cell cycle inhibitors such as *CDKN1A* and *CDKN2B* (data not shown). Additionally, PRMT6-deficient cells expressed more SSEA3 at their surface than their control counterparts, suggesting that, in absence of PRMT6, cells tend to retain their pluripotency state even after ATRA-induced differentiation. These findings conform with the observed cell cycle defects, since stem cells often show a low proliferation rate and a bias to quiescence (Glauche et al., 2009). Similarly, we observed reduced numbers of Pax6-positive and proliferating neural progenitors, respectively, during murine neurogenesis *in vivo*. Altogether, our data reveal that PRMT6 loss promotes the pluripotency state and perturbs the proliferation as well as differentiation capacity of NT2/D1 cells and neural precursor cells in the developing mouse brain, indicating that PRMT6 contributes to these key biological processes.

ChIP-seq profiling using anti-H3R2me2a antibodies revealed that the H3R2me2a peaks detected in NT2/D1 cells were PRMT6-dependent, as shown by the strongly reduced or lost H3R2me2a enrichment in PRMT6 knockout cells. Although PRMT6 and PRMT4 have been found to possess partially overlapping substrate specificity in certain cell types, such as mouse embryonic fibroblasts, PRMT6 seems to be the predominant methyltransferase for H3R2 in NT2/D1 cells (Torres-Padilla et al., 2007). In previous studies, we and others found that H3R2me2a mainly contributes to gene repression and occurs at silent genes (Guccione et al., 2007; Hyllus et al., 2007; Iberg et al., 2008). Intriguingly, we identified here that H3R2me2a is primarily deposited at active genes in NT2/D1 cells, both at promoter and enhancer sites. This apparent discrepancy is likely due to the fact that the hitherto-existing knowledge was predominantly obtained from analyses of individual genes and lacked unbiased genome-wide approaches to map the PRMT6-dependent H3R2me2a deposition as well as its cross talk with neighboring histone marks. Our attempts to also identify the PRMT6 binding sites in NT2/D1 cells by ChIP-seq unfortunately failed. All currently commercially available and in-house-generated PRMT6 antibodies did not efficiently immunoprecipitate PRMT6 from chromatin. Based on these observations and the fact that our in-house-generated antibodies showed specific though weak enrichment of chromatin-bound PRMT6 (Hyllus et al., 2007; Stein et al., 2012, 2016), we conclude that PRMT6 is a very dynamic nuclear protein, which transiently interacts with chromatin and therefore might escape detection, even when using double-cross-linking ChIP strategies.

Our analysis of the PRMT6-dependent transcriptome in NT2/D1 cells showed that 25% of deregulated genes associate with H3R2me2a binding sites in their proximity and are regarded as direct targets of H3R2me2a. Strikingly, the majority of these genes were downregulated, indicating a predominant transcriptional activating function of the mark. These findings are in agreement with studies reporting an activating role of PRMT6, e.g., in nuclear hormone receptor-dependent transcription (Harrison et al., 2010). The remaining genes, which are not marked by H3R2me2a, but show an altered transcriptional output upon PRMT6 deletion, are likely regulated by different mechanisms. This notion is in agreement with the findings that PRMT6 methylates several other substrates at the chromatin, for example, histone H3 at other arginines (H3R42), other histones (H2A, H4), and transcription factors (Casadio et al., 2013; Herglotz et al., 2013; Hyllus et al., 2007; Waldmann et al., 2011). Additionally, non-catalytic functions of PRMT6 and indirect mechanisms might account for transcriptional deregulation of these H3R2me2a-independent target genes. For example, *CDKN1A*, which has been shown to be a direct target of H3R2me2a in several human cell lines (Kleinschmidt et al., 2012; Phalke et al., 2012; Stein et al., 2012), does not show any enrichment of the mark in its promoter or enhancer region in NT2/D1 cells, despite being upregulated in the absence of PRMT6 (data not shown). Interestingly, the transcription factor MITF, which has been reported to activate *CDKN1A* expression (Carreira et al., 2005), is a downregulated and direct H3R2me2a target gene in NT2/D1 cells and hence might be responsible for the enhanced *CDKN1A* transcript levels in PRMT6 knockout cells.

Our analysis of the gene-regulatory role of H3R2me2a at promoter and enhancer sites uncovered further unexpected insights. This mark seems to execute opposing transcriptional effects depending on its genomic location: repressive functions at promoters and activating functions at enhancers (Figure 7). Promoter-bound H3R2me2a co-localizes with high H3K4me3 occupancy and antagonizes the deposition of this well-known active promoter mark, likely by interfering with the recruitment of KMT2A. This results in a diminished transcriptional activity of target genes. Our findings extend the understanding on the previously reported repressive nature of H3R2me2a, since this rather occurs at active genes than at silent gene loci, causing a restraint of their transcriptional output (Guccione et al., 2007; Hyllus et al., 2007; Iberg et al., 2008). PRMT6, potentially via H3R2me2a deposition at gene promoters, leads to fine-tuning of the transcriptional program in NT2/D1 cells and impedes unauthorized high expression of pluripotency genes as well as differentiation-associated genes (Figure 7A). In contrast, non-promoter H3R2me2a peaks co-localize with active enhancer marks, such as H3K4me1 and H3K27ac. Here, H3R2me2a might positively influence the deposition of these two enhancer marks, possibly by recruitment of KMT2D (subsequently p300), and thereby contributes to transcriptional activation of the associated genes (Figure 7B). At both locations, promoter as well as enhancer sites, H3R2me2a seems to modulate the deposition of adjacent histone marks, in agreement with the concept that arginine methylation exerts its regulatory activity by facilitating or diminishing protein-protein interactions. Whether H3R2me2a is sufficient and thereby decisive for regulating the chromatin recruitment of KMT2A and KMT2D requires further investigations in the future. Collectively, we conclude that PRMT6, likely via its catalytic activity and H3R2me2a, regulates the

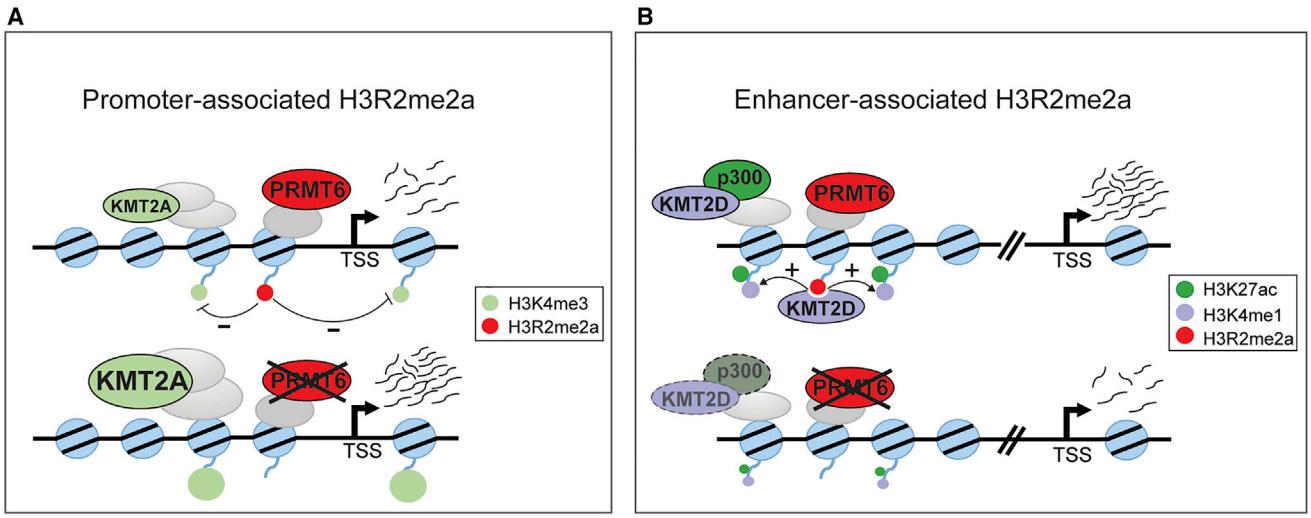

Figure 7. Model for the PRMT6-Dependent Deposition and Function of H3R2me2a at Promoter and Enhancer Sites

(A) Promoter-deposited H3R2me2a peaks (red circles) occur in proximity to the TSS of target genes, which are concomitantly marked with high H3K4me3 occupancy (green circles). These H3R2me2a binding sites associate with genes of medium to high expression levels. Here, PRMT6, potentially via H3R2me2a, diminishes the transcriptional output of target genes by counteracting KMT2A/H3K4me3 (upper panel). Deletion of PRMT6 and concomitant loss of H3R2me2a lead to increased binding of KMT2A as well as increased occupancy of H3K4me3 (as illustrated by the larger green circles) and unauthorized high expression of pluripotency and differentiation-associated genes (lower panel).

(B) Enhancer-deposited H3R2me2a (red circles) co-localizes with the active enhancer marks H3K4me1 and H3K27ac (purple and green circles, respectively). Here, PRMT6, potentially via H3R2me2a, enhances the transcriptional output of target genes by positively influencing the deposition of H3K4me1/H3K27ac, possibly through recruitment of KMT2D and subsequently p300 (upper panel). Deletion of PRMT6 and concomitant loss of H3R2me2a coincide with decreased binding of KMT2D as well as occupancy of H3K4me1/H3K27ac (as illustrated by the smaller circles) and impaired differentiation-dependent transcriptional activation of these important target genes (lower panel).

transcriptional output of genes relevant for neural differentiation through opposing effects on promoter and enhancer activities (Figure 7).

EXPERIMENTAL PROCEDURES

Cell Lines and Reagents

NT2/D1, U2OS, HeLa, and HEK293T cells were maintained in DMEM supplemented with 10% fetal calf serum (FCS) (Gibco-BRL) and 1% penicillin/streptomycin at 37°C and 5% CO_2. Neural differentiation of NT2/D1 cells was induced with 1 μM ATRA (Sigma) according to the protocol of Andrews (1984). MS049 hydrochloride was purchased from Sigma (SML15530). Detailed information on antibodies and plasmids is supplied in Supplemental Experimental Procedures.

Production of Lentiviral Particles and Infection of Cells

For CRISPR/Cas9-mediated deletion of *PRMT6* in NT2/D1 and U2OS cell as well as doxycycline-inducible expression of PRMT6 in NT2/D1 KO cells, HEK293T cells were transfected with packaging plasmids and lentiviral expression plasmids. Subsequently, lentiviral particles were used for cell infection as described in Supplemental Experimental Procedures.

Synthetic Histone Peptides

Unmodified and modified N-terminal histone peptides followed by a C-terminal cysteine residue or biotin moiety were obtained from Peptide Specialty Laboratories (Heidelberg, Germany). Modified peptides were synthesized by using either monomethylated, asymmetrically dimethylated, symmetrically dimethylated arginine, or mono-, di-, trimethylated lysine. Dot blot analysis and peptide pull-downs were performed as described in Supplemental Experimental Procedures.

Flow Cytometry

For quantification of the cell cycle distribution as well as pluripotency marker analysis, flow cytometry was used as described in Supplemental Experimental Procedures.

Animals

Constitutive *Prmt6* −/− (KO) mice were provided by the laboratory of Stephane Richards (Neault et al., 2012). For generation of $Prmt6^{-/-}$ (KO), $Prmt6^{+/-}$ (HET), and $Prmt6^{+/+}$ (WT) embryos of E12.5, pregnant female mice (*Prmt6* HET) were sacrificed by cervical dislocation, and embryos were decapitated. Killing of mice for tissue preparation was as approved by the animal protection commissioner of the University of Marburg. Tissue preparation and analysis are described in detail in Supplemental Experimental Procedures.

RNA Isolation, RT-qPCR, and RNA-Seq

RT-qPCR and RNA-seq were performed as described in Supplemental Experimental Procedures.

ChIP-qPCR and ChIP-Seq

For immunoprecipitation of histone marks, cells were cross-linked with 1% formaldehyde, whereas for immunoprecipitation of histone modifiers additionally disuccinimidyl glutarate (DSG) was used. ChIP experiments and detailed settings of genomic analyses are described in Supplemental Experimental Procedures.

Statistical Analysis

All experiments were performed at least three times (biological replicates). Reproducible and representative datasets are shown. Corresponding statistical tests are mentioned in the figure legends. Error bars represent mean ± SD of triplicate measurements.

DATA AND SOFTWARE AVAILABILITY

The accession number for the ChIP-seq and RNA-seq data reported in this paper is GEO: GSE107612.

SUPPLEMENTAL INFORMATION

Supplemental Information includes Supplemental Experimental Procedures and eight figures and can be found with this article online at https://doi.org/10.1016/j.celrep.2018.08.052.

ACKNOWLEDGMENTS

We thank all members of the U.-M.B. laboratory for their support during the work progress and Inge Sprenger and Christiane Rohrbach for technical assistance. We are grateful to Sophie Meyer and Felix Schneider for their support in murine brain analyses. We thank Stéphane Richard for providing the *Prmt6*$^{-/-}$ mouse model to us. This work was funded by DFG (Deutsche Forschungsgemeinschaft) Grants TRR81 A03, SFB1213 A05, BA 2292/1, and BA 2292/4 (to U.-M.B.) and GRK1213 and RU 1232/7-1 (to M.B.R.) and by Deutsche José Carreras Leukämie-Stiftung e.V. Grant DJCLS R 13/17 (to U.-M.B.).

AUTHORS CONTRIBUTIONS

C.B., P.S., M.M., R.R.N., G.H.-S., and A.N. performed experiments. E.K., R.F., and S.S.P. generated reagents. C.B., P.S., M.M., M.B.R., G.H.-S., F.F., M.B., T.S., S.P., and U.-M.B. analyzed data. U.-M.B. supervised. C.B. and U.-M.B. wrote the paper.

DECLARATION OF INTERESTS

The authors declare no competing interests.

Received: December 28, 2017
Revised: July 19, 2018
Accepted: August 17, 2018
Published: September 18, 2018

REFERENCES

Andrews, P.W. (1984). Retinoic acid induces neuronal differentiation of a cloned human embryonal carcinoma cell line in vitro. Dev. Biol. *103*, 285–293.

Barski, A., Cuddapah, S., Cui, K., Roh, T.Y., Schones, D.E., Wang, Z., Wei, G., Chepelev, I., and Zhao, K. (2007). High-resolution profiling of histone methylations in the human genome. Cell *129*, 823–837.

Calo, E., and Wysocka, J. (2013). Modification of enhancer chromatin: what, how, and why? Mol. Cell *49*, 825–837.

Carreira, S., Goodall, J., Aksan, I., La Rocca, S.A., Galibert, M.D., Denat, L., Larue, L., and Goding, C.R. (2005). Mitf cooperates with Rb1 and activates p21Cip1 expression to regulate cell cycle progression. Nature *433*, 764–769.

Casadio, F., Lu, X., Pollock, S.B., LeRoy, G., Garcia, B.A., Muir, T.W., Roeder, R.G., and Allis, C.D. (2013). H3R42me2a is a histone modification with positive transcriptional effects. Proc. Natl. Acad. Sci. USA *110*, 14894–14899.

Damez-Werno, D.M., Sun, H., Scobie, K.N., Shao, N., Rabkin, J., Dias, C., Calipari, E.S., Maze, I., Pena, C.J., Walker, D.M., et al. (2016). Histone arginine methylation in cocaine action in the nucleus accumbens. Proc. Natl. Acad. Sci. USA *113*, 9623–9628.

Dhar, S.S., Lee, S.H., Kan, P.Y., Voigt, P., Ma, L., Shi, X., Reinberg, D., and Lee, M.G. (2012). Trans-tail regulation of MLL4-catalyzed H3K4 methylation by H4R3 symmetric dimethylation is mediated by a tandem PHD of MLL4. Genes Dev. *26*, 2749–2762.

Dhawan, S., Georgia, S., Tschen, S.I., Fan, G., and Bhushan, A. (2011). Pancreatic β cell identity is maintained by DNA methylation-mediated repression of Arx. Dev. Cell *20*, 419–429.

Gayatri, S., and Bedford, M.T. (2014). Readers of histone methylarginine marks. Biochim. Biophys. Acta *1839*, 702–710.

Glauche, I., Moore, K., Thielecke, L., Horn, K., Loeffler, M., and Roeder, I. (2009). Stem cell proliferation and quiescence—two sides of the same coin. PLoS Comput. Biol. *5*, e1000447.

Guccione, E., Bassi, C., Casadio, F., Martinato, F., Cesaroni, M., Schuchlautz, H., Lüscher, B., and Amati, B. (2007). Methylation of histone H3R2 by PRMT6 and H3K4 by an MLL complex are mutually exclusive. Nature *449*, 933–937.

Harrison, M.J., Tang, Y.H., and Dowhan, D.H. (2010). Protein arginine methyltransferase 6 regulates multiple aspects of gene expression. Nucleic Acids Res. *38*, 2201–2216.

Herglotz, J., Kuvardina, O.N., Kolodziej, S., Kumar, A., Hussong, H., Grez, M., and Lausen, J. (2013). Histone arginine methylation keeps RUNX1 target genes in an intermediate state. Oncogene *32*, 2565–2575.

Houldsworth, J., Heath, S.C., Bosl, G.J., Studer, L., and Chaganti, R.S.K. (2002). Expression profiling of lineage differentiation in pluripotential human embryonal carcinoma cells. Cell Growth Differ. *13*, 257–264.

Hyllus, D., Stein, C., Schnabel, K., Schiltz, E., Imhof, A., Dou, Y., Hsieh, J., and Bauer, U.-M. (2007). PRMT6-mediated methylation of R2 in histone H3 antagonizes H3 K4 trimethylation. Genes Dev. *21*, 3369–3380.

Iberg, A.N., Espejo, A., Cheng, D., Kim, D., Michaud-Levesque, J., Richard, S., and Bedford, M.T. (2008). Arginine methylation of the histone H3 tail impedes effector binding. J. Biol. Chem. *283*, 3006–3010.

Kirmizis, A., Santos-Rosa, H., Penkett, C.J., Singer, M.A., Vermeulen, M., Mann, M., Bähler, J., Green, R.D., and Kouzarides, T. (2007). Arginine methylation at histone H3R2 controls deposition of H3K4 trimethylation. Nature *449*, 928–932.

Kleinschmidt, M.A., de Graaf, P., van Teeffelen, H.A., and Timmers, H.T. (2012). Cell cycle regulation by the PRMT6 arginine methyltransferase through repression of cyclin-dependent kinase inhibitors. PLoS One *7*, e41446.

Lee, V.M., and Andrews, P.W. (1986). Differentiation of NTERA-2 clonal human embryonal carcinoma cells into neurons involves the induction of all three neurofilament proteins. J. Neurosci. *6*, 514–521.

Lee, Y.H., Ma, H., Tan, T.Z., Ng, S.S., Soong, R., Mori, S., Fu, X.Y., Zernicka-Goetz, M., and Wu, Q. (2012). Protein arginine methyltransferase 6 regulates embryonic stem cell identity. Stem Cells Dev. *21*, 2613–2622.

McKee, A.E., Minet, E., Stern, C., Riahi, S., Stiles, C.D., and Silver, P.A. (2005). A genome-wide in situ hybridization map of RNA-binding proteins reveals anatomically restricted expression in the developing mouse brain. BMC Dev. Biol. *5*, 14.

Michaud-Levesque, J., and Richard, S. (2009). Thrombospondin-1 is a transcriptional repression target of PRMT6. J. Biol. Chem. *284*, 21338–21346.

Neault, M., Mallette, F.A., Vogel, G., Michaud-Levesque, J., and Richard, S. (2012). Ablation of PRMT6 reveals a role as a negative transcriptional regulator of the p53 tumor suppressor. Nucleic Acids Res. *40*, 9513–9521.

Phalke, S., Mzoughi, S., Bezzi, M., Jennifer, N., Mok, W.C., Low, D.H., Thike, A.A., Kuznetsov, V.A., Tan, P.H., Voorhoeve, P.M., and Guccione, E. (2012). p53-Independent regulation of p21Waf1/Cip1 expression and senescence by PRMT6. Nucleic Acids Res. *40*, 9534–9542.

Rosenfeld, J.A., Wang, Z., Schones, D.E., Zhao, K., DeSalle, R., and Zhang, M.Q. (2009). Determination of enriched histone modifications in non-genic portions of the human genome. BMC Genomics *10*, 143.

Shen, Y., Szewczyk, M.M., Eram, M.S., Smil, D., Kaniskan, H.Ü., de Freitas, R.F., Senisterra, G., Li, F., Schapira, M., Brown, P.J., et al. (2016). Discovery of a potent, selective, and cell-active dual inhibitor of protein arginine methyltransferase 4 and protein arginine methyltransferase 6. J. Med. Chem. *59*, 9124–9139.

Stein, C., Riedl, S., Rüthnick, D., Nötzold, R.R., and Bauer, U.M. (2012). The arginine methyltransferase PRMT6 regulates cell proliferation and senescence through transcriptional repression of tumor suppressor genes. Nucleic Acids Res. *40*, 9522–9533.

Stein, C., Nötzold, R.R., Riedl, S., Bouchard, C., and Bauer, U.M. (2016). The arginine methyltransferase PRMT6 cooperates with polycomb proteins in regulating HOXA gene expression. PLoS One *11*, e0148892.

Torres-Padilla, M.E., Parfitt, D.E., Kouzarides, T., and Zernicka-Goetz, M. (2007). Histone arginine methylation regulates pluripotency in the early mouse embryo. Nature *445*, 214–218.

Waldmann, T., Izzo, A., Kamieniarz, K., Richter, F., Vogler, C., Sarg, B., Lindner, H., Young, N.L., Mittler, G., Garcia, B.A., and Schneider, R. (2011). Methylation of H2AR29 is a novel repressive PRMT6 target. Epigenetics Chromatin *4*, 11.

Wang, C., Lee, J.-E., Lai, B., Macfarlan, T.S., Xu, S., Zhuang, L., Liu, C., Peng, W., and Ge, K. (2016). Enhancer priming by H3K4 methyltransferase MLL4 controls cell fate transition. Proc. Natl. Acad. Sci. USA *113*, 11871–11876.

Wang, S.P., Tang, Z., Chen, C.W., Shimada, M., Koche, R.P., Wang, L.H., Nakadai, T., Chramiec, A., Krivtsov, A.V., Armstrong, S.A., and Roeder, R.G. (2017). A UTX-MLL4-p300 transcriptional regulatory network coordinately shapes active enhancer landscapes for eliciting transcription. Mol. Cell *67*, 308–321.e6.

Yang, Y., and Bedford, M.T. (2013). Protein arginine methyltransferases and cancer. Nat. Rev. Cancer *13*, 37–50.